International Journal of GEOMATE, April., 2021, Vol.20, Issue 80, pp135-142
ISSN: 2186-2982 (P), 2186-2990 (O), Japan, DOI: https://doi.org/10.21660/2021.80.j2044
Geotechnique, Construction Materials and Environment

A LOW-COST UAV BASED APPLICATION FOR IDENTIFY AND MAPPING A GEOTHERMAL FEATURE IN IE JUE MANIFESTATION, SEULAWAH VOLCANO, INDONESIA

Marwan[1], Rinaldi Idroes[2], Muhammad Yanis*[1], Ghazi Mauer Idroes[3], Syahriza[4]

[1]Department of Geophysical Engineering, Faculty of Engineering, Universitas Syiah Kuala, Indonesia
[2]Department of Chemistry, Faculty of Mathematics and Natural Sciences, Universitas Syiah Kuala, Indonesia
[3]Department of Chemical Engineering, Faculty of Engineering, Universitas Syiah Kuala, Indonesia
[4]Department of Mechanical Engineering, Faculty of Engineering, Universitas Syiah Kuala, Indonesia

*Corresponding Author, Received: 02 Dec. 2020, Revised: 11 Jan. 2021, Accepted: 06 Feb. 2021

ABSTRACT: Mt. Seulawah Agam could make a good location for a geothermal power plant with an estimated energy of 150 Mwe. In geothermal exploration, thermal and multispectral imagery is required for surface temperature calculation, subsurface temperature modeling, and mapping of geothermal potential in volcanoes. In general, temperature data and vegetation index are obtained through such satellite images as Landsat, MODIS, and Sentinel. However, satellite images cannot be used for a small area due to the low resolution (> 15 m/px). In this study, the researchers used a small DJI Phantom 4 Quadcopter equipped with the FLIR One and MAPIR Survey 3 sensors to map the heat signatures of a geothermal feature from the Ie Jue geothermal manifestation, Seulawah Agam, Indonesia. An area of 500 m x 430 m has been scanned, and the images were mosaicked and processed using Drone Deploy Cloud and ArcGIS 10.2. Based on the data processing, NDVI data calculated from the MAPIR sensor are capable of showing vegetation contrast with high resolution (5 cm/px) in several manifestations, which also correspond to Landsat-8 imagery. Meanwhile, the FLIR thermal sensor shows a temperature of 85 °C in the manifestation area, which was confirmed by a geo-thermometer and field outcrops. It was proved that, compared to satellite imagery, UAVs could be applied effectively to support the quantitative assessment of geothermal resources in volcanoes.

Keywords: UAV, Thermal infrared imaging, Geothermal, Aerial monitoring.

1. INTRODUCTION

Geothermal is one of the untapped potentials in alternative energy sources that Indonesia could benefit from. It is estimated that Indonesia has 40% of the world's total geothermal potential, or around 28,617 MWe [1,2], which could replace fossil energy and is environmentally friendly [3]. In addition to its use for power plants, geothermal has been developed to support the community's economy through geo-tourism [4]. Located at the northern tip of Sumatra Island, the Aceh Province has three Type-A active volcanoes. One of the volcanoes is Mt. Seulawah Agam in Aceh Besar (Fig. 1), which could make a good location for geothermal power plants. In order to utilize this energy source, a comprehensive range of earth science studies is needed [5]. Satellite remote sensing is an important part of current volcanology, especially to explore and monitor geothermal systems and potentials [6,7]. This is due to the availability of satellite image data for a long period of time and with a large area coverage so that it can be used for monitoring thermal activity and estimating energy potential in volcanic areas [8]. Although satellite imagery is widely applied, several factors prevent optical imagery, such as the Landsat series from working correctly [9]. In tropical regions like Indonesia, those factors include the presence of huge amounts of clouds, which interfere with the interpretation of geothermal features. In addition, the smaller size of craters and areas of manifestation make satellite data with a resolution of 15-30 m/px almost unusable. Therefore, surface temperature data from satellite imagery often differ from temperatures from in-situ geochemical measurements.

Another monitoring practice, airborne high-resolution, has proven to be an effective method to substitute satellite imagery in mapping geothermal features of volcanoes. This method has been widely applied for geothermal monitoring in various volcanoes in the world [10–12]. Both cost and dynamic mobility for aerial surveying could be minimized substantially if an unmanned aerial vehicle (UAV) as a low-cost platform is used to replace airplanes. In this study, DJI Quad copter Drone Phantom 4 was used to study geothermal features in the Ie Jue manifestation area on Seulawah Agam volcano in the form of hot springs and warm ground. As the drone is small, the load-carrying capacity, wind resistance, and drone range have imposed a payload limit compared to a manned aircraft. Therefore, the researchers used the

light-weight FLIR One and multispectral Survey 3 thermal sensors from MAPIR to be mounted to and carried by the DJI Phantom 4. The research highlights a cost-effective method for collecting TIR and multispectral images using UAV and demonstsrating an efficient workflow for processing and analyzing the collected data.

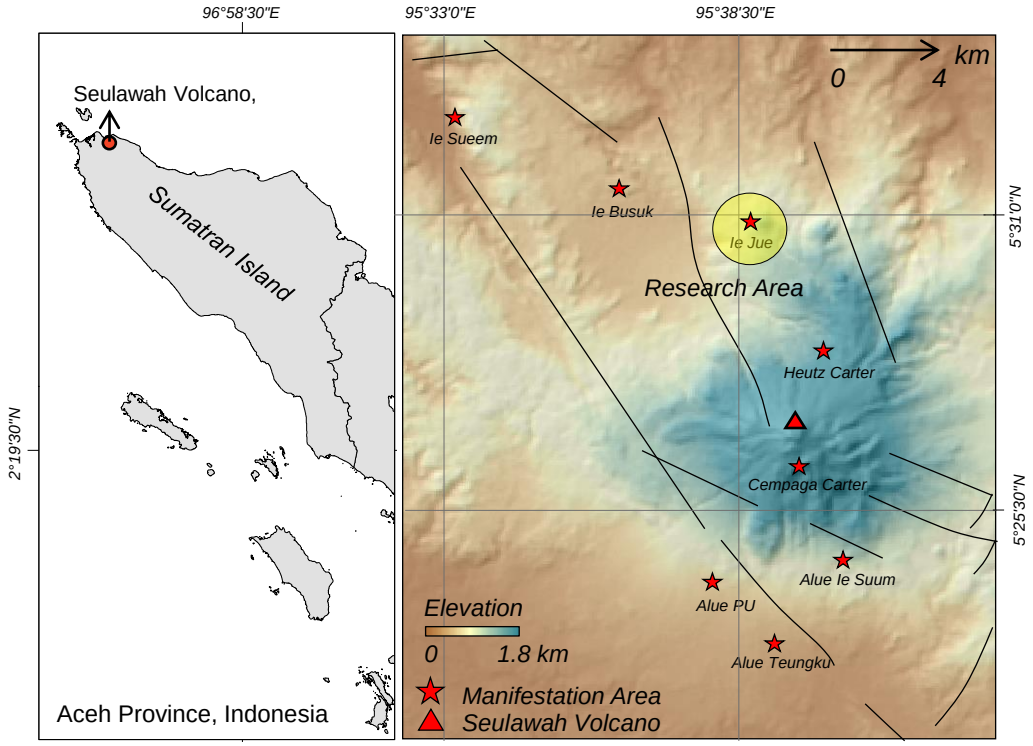

Fig.1 The aerial monitoring location in the manifestation area in Ie Jue, Aceh Besar. The distribution of the manifestations is generally close to the fault that controls the rise of the fluid to the surface. Mt. Seulawah Agam has eight geothermal manifestations [1,13], two of which are craters measured 200 x 200 m, and the other six include hot springs and warm ground with smaller areas [14].

2. SEULAWAH AGAM GEOTHERMAL SYSTEM

Located in Aceh Besar Regency of the Province of Aceh, Indonesia, Mt. Seulawah Agam is of stratovolcanic type. In general, the geology of Seulawah Agam is dominated by LamTeuba rocks. These formations consist of basalt, andesite to dacite, pumice breccia, tuff, agglomerates, and dust flows [15]. Seulawah Agam has several surface manifestations, including one in the south, close to the top of the volcano, namely the Ceumpaga Crater, and the other in the north, the Heutsz Crater. The area also hosts several hot springs, especially in the Ie Suum [13] and Ie Jue [14] areas. The manifestation in the Ie Jue area is characterized by the presence of warm ground, steaming ground, hot springs, fumaroles, and mud puddles. Studies into the water geothermometer showed that the water temperature of the Ie Jue manifestation is 472.4 ± 91.4°C [1,14].

Tectonically, Mt. Seulawah Agam is controlled by the Great Sumatran Fault, which stretches 1,700 km from Lampung through the Andaman Sea [2]. This fault is divided into 20 segments [16,17], where Seulawah Agam is located close to the Seulimum segment leading up to Aceh Island. Fig. 1 shows some of the local fault distribution in Mt. Seulawah Agam [18,19]. The results of geophysical exploration using magnetotelluric [20] and transient electromagnetic [18] have provided information on the depth of the main system of the Seulawah Agam volcano, namely, the caprock zone at a depth of 1 km, the reservoir at 2 km, and the heat source at 3 km below the surface. The VLF-EM and magnetic data [20] also show a near structure of the faults in the depth of 10 m as the main control in Ie Jue manifestation.

3. MATERIAL AND METHODS

To analyze the geothermal features at Ie Jue manifestation of Seulawah Agam, the researchers used Landsat 8 satellite image data and several sensors installed on the drone as additional payloads for thermal and multispectral data. The two were then compared with optical image analysis from the Landsat Series. The drone used in this study is DJI

Phantom 4 with a weight of 1.38 kg and a coverage range of up to 5 km, and a maximum flight time of 30 minutes per one battery. It is equipped with an RGB camera with a 20-megapixel resolution capable of taking photos and videos. Each image is tagged with a GPS, which provides information such as its latitude and longitude as well as the altitude at which it was taken.

To obtain multispectral data, the MAPIR Survey 3 camera was integrated into the DJI Phantom 4 with the addition of a standard mounting and GPS from MAPIR Inc., as shown in fig.2. This sensor allows for Near-infrared (NIR) image capture because it is composed of different bands, namely, green with a wavelength of 550 nm, red 660 nm, and near-infrared with a wavelength of 850 nm. Multispectral data from MAPIR Survey 3 was used to calculate the normalized difference vegetation index (NDVI) using the equation commonly used for satellite image data as shown in Eq. (1):

$$NDVI = \left(\frac{R_{NIR}-R_{RED}}{R_{NIR}+R_{RED}}\right) \quad (1)$$

Where R_{NIR} is the reflectance of the near-infrared band, and R_{RED} is the reflectance of the red band. In addition to calculating vegetation that shows stress due to temperature anomalies in geothermal areas, the NDVI value is needed to calculate the proportion of vegetation (PV), defined as the ratio of the vertical projection over the vegetation canopy in each pixel as follows in Eq. (2):

$$PV = \left(\frac{NDVI-NDVIs}{NDVIv-NDVIv}\right)^2 \quad (2)$$

Where $NDVI_s$ is response value on vacant land, and $NDVI_v$ is response value on the densely-vegetated area. Then, from the data of vegetation propagation, the parameter of land surface emissivity (LSE) is calculated, which is the ratio of radiation energy emitted by the ground surface to radiation emitted by black bodies at the same temperature, which can be expressed mathematically in Eq. (3):

$$\varepsilon = 0.004\, PV + 0.986 \quad (3)$$

As MAPIR sensor cannot map temperature, the researchers added a FLIR One thermal camera with a pixel size of 17µm, 8-14µm spectral range, and an accuracy of up to ± 3°C. This sensor can work in a temperature range from 5 - 120°C.

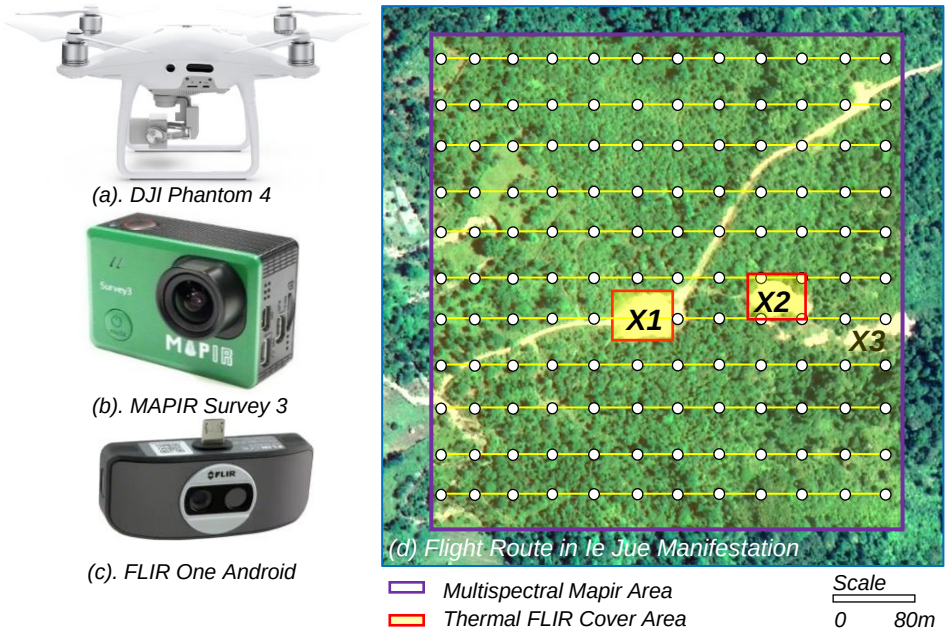

Fig.2 The equipment and sensors used in this study, (a) DJI Phantom 4 as a quadcopter drone type UAV, (b) MAPIR Survey 3, (c) a FLIR One sensor to measure surface temperature. Meanwhile, (d) is a flight route that shows the difference in the coverage area for the multispectral and thermal sensors.

This FLIR One camera takes pictures in a digital format with a resolution of 640 x 480 per frame. Fig. 2 shows the equipment for mapping the geothermal features in Ie Jue manifestation. The researchers applied different flight route cover for the two sensors. The MAPIR covered the entire location with an area of 500 m x 430 m as shown in the yellow line, and FLIR One was only focused on a few hot spring outcrop locations such as X_1 with an area of 30 x 35 m and X_2 with an area of 2 x 2 m. The symbols of X_1, X_2, and X_3 in the image represent the outcrop locations of manifestations such as warm ground, hot springs, and the un-vegetated area, which characterize the volcanic activity below

the surface. The researchers used Drone Deploy software to control the shooting, which allows for overlapping, speed, height, and area measurement settings. The images were collected using the single grid option from the autopilot software with up to 80% overlapping, as shown in Fig. 2.d.

4. RESULT AND DISCUSSION

4.1 Satellite Data

The researchers used Landsat 8 Collection Level-2 data on 29 January 2019 to validate multispectral and thermal data on the UAV system. The data was obtained from Earth Explorer USGS with geometry correction applied to the images. Landsat 8 consists of five Visual near Infra-Red (VNIR) bands, two Short Wave Infrared (SWIR) bands, 1 panchromatic band, 1 band for cirrus cloud detection, and 2 Thermal Infrared (TIR) bands. To obtain NDVI and surface temperature, the optical image data has to go through several important processing stages, including radiometric correction, brightness temperature calculation, and emissivity calculation, as shown in the USGS User handbook. Fig. 3 shows some of the results of the processing and composite band on Landsat 8 data.

Geomorphological data calculated from the technique of RGB 5, 6, 7 composite band shows the lithological characteristics found in the Ie Jue manifestation area. Alluvium rocks with a smooth texture are indicated by light blue color, while dark colors are a response to volcanic minerals with a coarse texture. NDVI data also showed contrasting differences between the manifestation and the surrounding conditions, where locations X_1, X_2 and X_3 are characterized by a high NDVI with a range of 0.5 - 0.8 response to the un-vegetated areas due to subsurface thermal activity. Furthermore, the emissivity data calculated from the NDVI data also shows the same distribution of anomalies. Several spots where manifestations are located, are indicated by low emissivity in response to the ratio of radiation energy emitted by unhealthy soil surfaces. We also overlaid temperature data from the thermal band analysis corresponding to NDVI response and emissivity, where a soil temperature of 25°C was obtained in the manifestation areas. In comparison, other areas indicated a lower temperature of <23°C. In general, optical image data can provide initial results from geothermal features in the Ie Jue manifestation. However, the resolution of satellite data is very low (15-30 m), so that the response obtained in the manifestation location with a small area (100 x 100 m) is only represented by 3 pixels of data for the thermal band and 6 pixels for the multispectral band. Therefore, a UAV drone was deployed as a low-cost method to study geothermal features in a relatively small area.

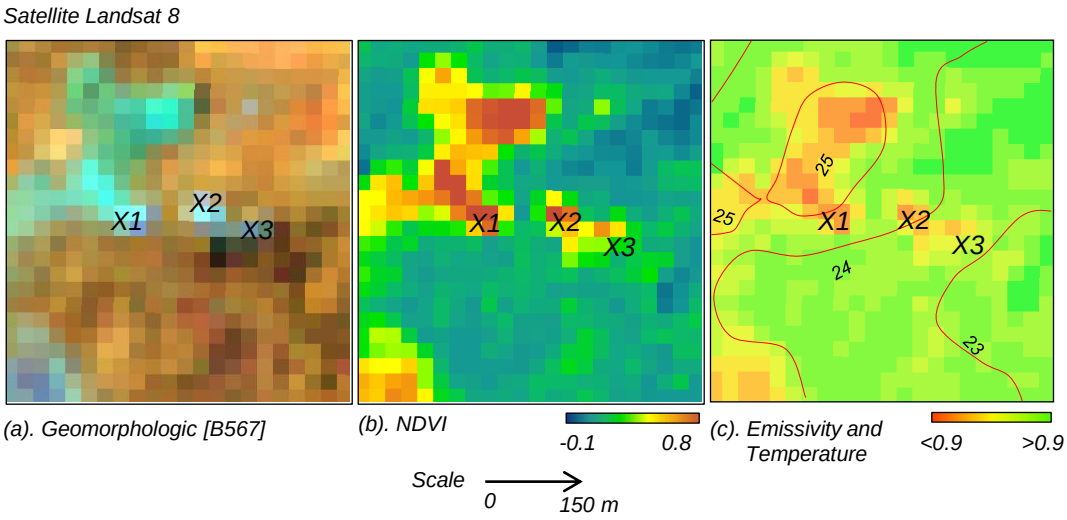

Fig.3 Analysis of satellite data at the location of Ie Jue manifestations. The Landsat OLI/TIRS data, accessed on 29 January 2019, was used to calculate (a) geomorphology through the composite band B 5, 6, 7; (b) NDVI; and (c) emissivity values obtained from vegetation propagation NDVI calculations. The data was also overlaid with the temperature contour obtained from the surface temperature from band 10 on Landsat 8.

4.2 Multispectral Image from MAPIR

The first step carried out on the multispectral data from MAPIR Survey 3 was mosaicking, from 734 files into one image file with a 5 cm/pixel resolution. The mosaicking process was carried out through the Drone Deploy Cloud on a trial basis so that Ortho-mosaic RGB data was obtained, as shown in Fig. 4.a. Then, RGB data in the form of a digital number is converted into reflectance so that calculations could be made to classify the NDVI data, as shown in Fig. 4.b. Finally, propagation

vegetation and emissivity data were calculated, as shown in Fig. 4.c. Ortho mosaic (RGB) data showed different color contrasts. For example, un-vegetated areas such as in X_1, X_2, and X_3 are characterized by yellow, while the purple color indicates vegetation areas. This ortho mosaic data can clearly distinguish the location of the manifestation area from the other because, in general, almost no vegetation is present on the manifestation areas due to the heat characteristic of volcanic activity, resulting in only a few types of plants that can grow on the spot. This ortho mosaic data is still in digital number, so it needs to be transformed into reflectance data to obtain NDVI values.

Quantifies vegetation can be carried out by looking at the difference ratio between the near-infrared band (which vegetation strongly reflects) and red band (which vegetation absorbs). Based on the NDVI map from the multispectral camera, the NDVI density classification generated a range of values between 0 - 0.49, where a high value indicates a denser area of vegetation and a lower value represents open areas or areas with no vegetation. A high NDVI value (0.3 - 0.49) was obtained in the area around the manifestations as a response to densely vegetated areas. Meanwhile, the manifestation areas showed lower NDVI values due to the un-vegetated areas, which indicates magmatic activity below the surface as a significant component in a geothermal system formation.

Hot temperatures from volcanic activity prevented some plants from growing in the manifestation area. It should be noted that the un-vegetated area was not only due to volcanic activity underneath but also due to farming activities by the communities, but in several locations such as on the north side of X_3 and the south side of X_2 and X_3, much lower NDVI values were obtained, which indicated a volcanic activity in the area. The same data is shown by the emissivity, where low values are obtained in some manifestation areas, and high values are obtained in areas where no outcrop from volcanic activity is present. This is because the surface emissivity data represents the ability of the land surface to convert heat energy into radiation energy so that the greater an object absorbs heat, the less the reflected radiation will be. Overall, this multispectral data produced the same vegetation distribution and emissivity responses as the Landsat 8 satellite data.

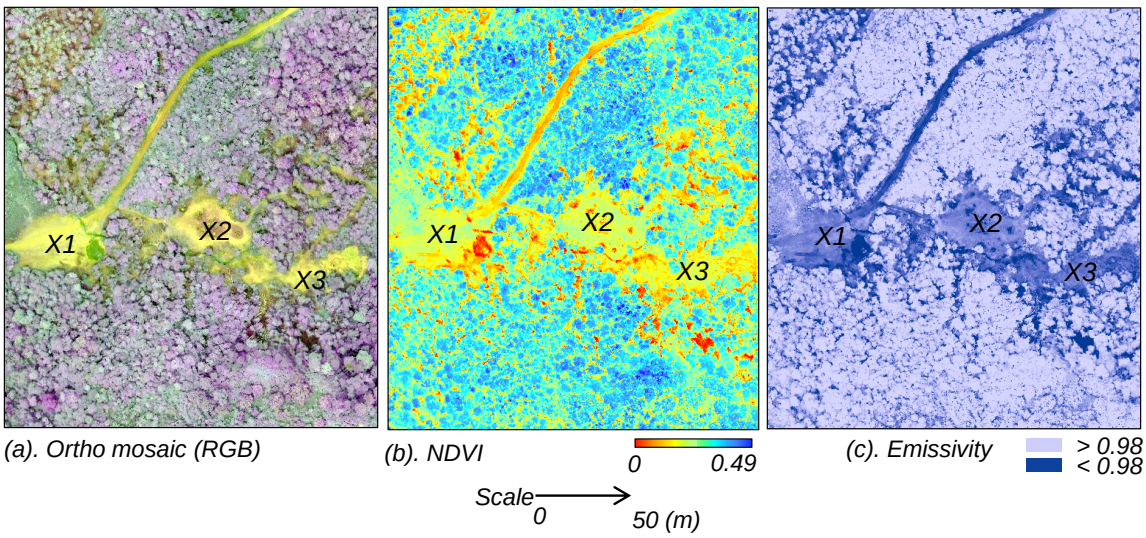

Fig.4 Data generated from the MAPIR Survey 3 multispectral camera; (a) original data as ortho mosaic in RGB which shows contrasting differences between vegetation areas and un-vegetated areas, (b) Classified NDVI data from red and green band calculations, and (c) emissivity data to show the ratio of energy emitted by the land surface.

4.3 Surface Temperature from FLIR One

FLIR thermal cameras provide data imaging modes in the form of 14-bit radiometric PNG or TIFF format. The radiometric sensor can be converted to the temperature data in Celsius or Kelvin using FLIR Tools, which is possible freely accessible on the FLIR website. The FLIR Tools is open-source software that allows importing, extracting to txt data, editing, visualizing, analyzing the images, and performing radiometric calibrations to the temperature data. However, only radiometric JPEG images with temperature data embedded in each pixel can be accessed with FLIR Tools and possibly converted to radiometrically in the CSV format. The temperature data file for each pixel from CSV is then visualized with MatLab using simple code for 2D data plotting. Fig. 5 shows the temperature distribution of X_1 compared to NDVI MAPIR in the Ie Jue manifestation, Seulawah

Agam, which confirms [21,22] that temperature data and NDVI can represent subsurface thermal activity on volcanoes.

The temperature data varies between 30-60 °C and is spread over several places and can be divided into three categories. Low temperature (<40 °C) was obtained on the east side, moderate temperature (<50 °C) was on the west side, and high value (> 50 °C) on the middle side westward. The overall temperature distribution of the FLIR One sensor is relatively the same as the NDVI MAPIR data response, but several anomalous responses were shown at several locations. For example, a high-temperature value is obtained on the west side, but NDVI data shows that the particular spot is a vegetated area. It indicates that even though the area is of low vegetation, the temperature at that location is relatively high as a response to the warm ground from the subsurface volcanic activity. The temperature distribution at several survey points is specifically presented in Table 1.

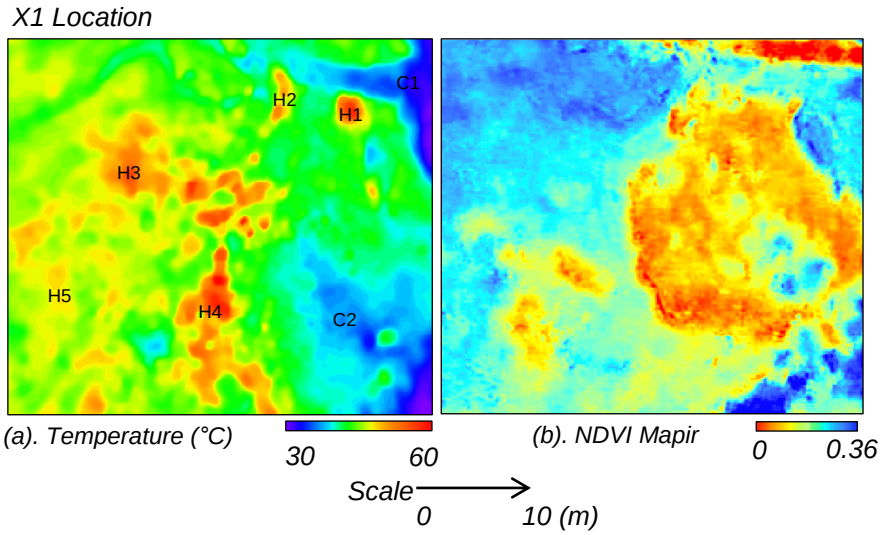

Fig.5 Comparison of the two sensors' responses at location X_1; (a) the temperature data in Celsius obtained by FLIR One, and (b) NDVI data from the multispectral sensor MAPIR Survey 3. The C symbol represents the cold area, and H represents the hot area of the measurement location.

Tabel 1. Comparison of temperature distribution from FLIR One with NDVI from MAPIR.

No	Location	Temperature Flir One (°C)	NDVI MAPIR	Description
1	C1	38.2	0.31	Vegetation area
2	H1	61.9	0.02	Hotspring
3	H2	55.2	0.05	Warm ground and close to the hotspring
4	H3	55.5	0.08	Warm groud
5	H4	61.4	0.20	Warm groud
6	H5	51.5	0.03	Warm groud
7	C2	38.8	0.25	Vegetation area

The highest temperature values were obtained at two locations, namely H1, with a temperature of 61.9 °C and H4, with a temperature of 61.4 °C. This is a response to the volcanic activity of Ie Jue manifestation, as confirmed by the hot spring in H1. A more interesting profile is found on H3. Although there is no hot spring above the surface, the location is characterized by a high temperature, indicating a response to the warm ground with thermal activity at a shallow depth. In other location where the hotspring is closed (H2), the temperature value was obtained at 55.2 °C which same as H3 temperature. This indicates that the location of H3 is the flow area of the hotspring below the surface. So we get a temperature that is relatively the same as H2 which is close to the hotspring location above the surface.

Meanwhile, in areas with dense vegetation (C1 and C2), the temperature value obtained is closer to the satellite data (38.8 °C). Due to the low data resolution for the thermal band, however, satellite data cannot provide accurate temperature information on relatively small manifestation areas.

Referring to geo-thermometer data measured in 2017, the temperature value at Ie Jue location X_1 is 98.62 °C. A relatively similar value was also obtained using the FLIR One sensor. The FLIR One thermal camera also scanned the X_2 location, which is only 50 m away from X_1, and where hot spring and warm ground outcrops are also located. However, due to technical problems with the UAV that failed to connect with the camera, we could only use a thermal camera at the height of 3 m through a climb to high topography so that the temperature distribution obtained was only in an area of 2 x 2 m, as shown in Fig. 6. The temperature distribution at this location varies from 30 to 85 °C, where a high-temperature distribution (50 - 85 °C) is obtained in most of the measurement area. This is a response to the hot spring located right on the west side (H1). Fig. 6.b is documentation of field outcrops in the form of hot springs.

Referring to geo-temperature data [1,14], the temperature on this spot is relatively the same; that is, 98.62 °C in the spring water material measured in 2017. The high-temperature value at this location indicates the volcanic activity of the Seulawah Agam volcano. Besides, the thermal map also shows low temperatures (<40 °C) on the east side (C1), which is a response to vegetated areas. This also corresponds to the NDVI MAPIR and Landsat 8 data, where high values dominate the east side in response to dense vegetation.

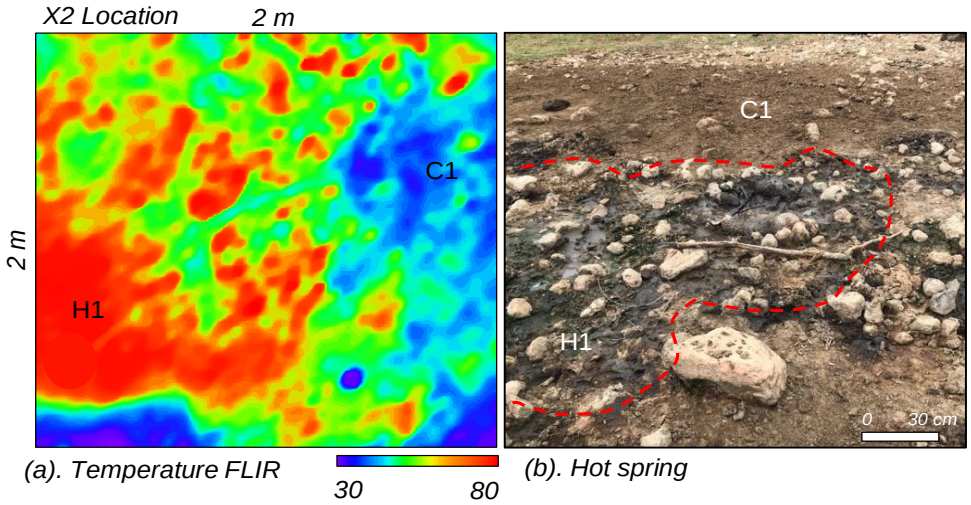

Fig.6 (a) is the temperature distribution data from the FLIR One sensor at location X_2, and (b) is one of the hot spring outcrops at the Ie Jue location, Aceh Besar. The red dotted line represents the hot spring area.

5. CONCLUSIONS

Temperature and NDVI data can show the volcanic activity from a volcano, but in tropical regions like Indonesia, optical satellite imagery is often blocked by clouds. On the other hand, free access optical images generally have a low resolution (> 15 m), making them practically unusable to study volcanoes or manifestations in relatively small areas such as in Ie Jue. Furthermore, we applied a low-cost UAV consisting of a quad copter drone from the DJI Phantom 4 Pro equipped with a multispectral camera from MAPIR Survey 3, and a FLIR One with a special mounting from MAPIR Inc. Based on the data processing, NDVI and thermal maps obtained from the UAV show a response that is relatively the same as the conventional Landsat-8 data. NDVI data from MAPIR show three un-vegetated areas, which are the responses to volcanic traces on the surface, such as hot spring and warm ground. Meanwhile, the thermal data from FLIR One show high temperatures obtained at several locations where hot springs and warm ground are identified, and the FLIR data correspond to those from geo-temperature measurements. Based on the results, it is concluded that the quad copter drone, to which several special sensors were mounted, shows vast potential for use in the study of volcanic activity at a lower cost, less time consuming, and high data resolution levels. Based on data processing, the UAV quad copter with MAPIR Survey 3 and FLIR One sensor are potentially used to study geothermal prospecting, especially in manifestation with a relatively small area.

6. ACKNOWLEDGMENT

The authors thank Freddy Sapta Wirandha for his extensive help in drone data acquisition, GIS Laboratory at Universitas Syiah Kuala for their support in MAPIR Survey 3 sensor, and also thanks to physics department students in field observation. The research was conducted as a part of the H-Index 2020 research grant from Universitas Syiah Kuala by number No.81/UN11.2.1/PT.01.03/PNBP/2020.

7. REFERENCES

[1] Rinaldi I., Yusuf M., Saiful., Alatas M., Subhan., Muslem., Suhendra R., Idroes G. M., Marwan., Teuku I. M., Geochemistry Exploration and Geothermometry Application in the North Zone of Seulawah Agam, Aceh Besar District, Indonesia. Energies, vol. 12, no. 23, p. 4442, Nov. 2019.

[2] Hochstein M. P. and Sudarman S., History of geothermal exploration in Indonesia from 1970 to 2000. Geothermics, 2008.

[3] Domra J.K., Djongyang N.D., Raïdandi, P. Njandjock N., and Dadjé A., A review of geophysical methods for geothermal exploration. Renewable and Sustainable Energy Reviews. 2015

[4] Marwan, Yanis M., Muzakir Z., and Nugraha S. G., Application of QR codes as a new communication technology and interactive tourist guide in Jaboi, Sabang. in IOP Conference Series: Materials Science and Engineering, Apr. 2020, vol. 796, no. 1.

[5] Zhang L., Tianyao H., Qibin X., Liang Z., Xiangpan C., Magnetotelluric investigation of the geothermal anomaly in Hailin, Mudanjiang, northeastern China. J. Appl. Geophys.,vol 118, 2015

[6] Mia M.B, Nishijima J, and Fujimitsu Y,. xploration and monitoring geothermal activity using Landsat ETM+images. A case study at Aso volcanic area in Japan.. J. Volcanol. Geotherm. Res., 2014.

[7] Qin Q., Zhang N., Nan P, and Chai L., Geothermal area detection using Landsat ETM+ thermal infrared data and its mechanistic analysis-A case study in Tengchong, China. Int. J. Appl. Earth Obs. Geoinf., 2011

[8] Darge M.Y., Hailu B.T., Muluneh A.A., and Kidane T., Detection of geothermal anomalies using Landsat 8 TIRS data in Tulu Moye geothermal prospect, Main Ethiopian Rift. Int. J. Appl. Earth Obs. Geoinf., 2019

[9] Wulder M.A., Joanne W., Nelson R., Erik N., Nicholas C., Thomas H., Lidar sampling for large-area forest characterization: A review, Remote Sensing of Environment. 2012

[10] Coolbaugh M. F., Kratt C., Fallacaro A., Calvin M. M., and Taranik J. V., Detection of geothermal anomalies using Advanced Spaceborne Thermal Emission and Reflection Radiometer (ASTER) thermal infrared images at Bradys Hot Springs, Nevada, USA. Remote Sens. Environ., 2007.

[11] Mia M.B., Bromley C.J., and Fujimitsu Y., Monitoring Heat Losses Using Landsat ETM + Thermal Infrared Data: A Case Study in Unzen Geothermal Field, Kyushu, Japan. Pure Appl. Geophys., 2013.

[12] Zaini N., Irwandi I., Abdullah F., and Van D. M., Infrared spectroscopy characteristics of mount Sinabung volcanic materials, North Sumatra, Indonesia. 2019.

[13] Rinaldi I., Yusuf M., Alatas M., Subhan., Lala A., Suhendra M., Idroes G M., Marwan. Geochemistry of hot springs in the Ie Seu'um hydrothermal areas at Aceh Besar district, Indonesia, 2018.

[14] Rinaldi I., Yusuf M., Alatas M., Subhan., Lala A., Suhendra M, Idroes G M., Marwan. Geochemistry of Sulphate spring in the Ie Jue geothermal areas at Aceh Besar district, Indonesia, 2019.

[15] Bennet M., Doyle P., Larwood J., and Prosser C., Geology on your Doorstep. Geol. Soc. Publ. 270pp, 1996.

[16] Sieh K., and Natawidjaja D., Neotectonics of the Sumatran fault, Indonesia. J. Geophys. Res. Solid Earth, vol. 105, no. B12, pp. 28295–28326, Dec. 2000.

[17] Rizal M., Ismail N., Yanis M., Muzakir, and Surbakti M.S., The 2D resistivity modelling on north sumatran fault structure by using magnetotelluric data. IOP Conf. Ser. Earth Environ. Sci., vol. 364, p. 012036, Dec. 2019

[18] Marwan, Yanis M., Idroes R, and Ismail N. 2D inversion and static shift of MT and TEM data for imaging the geothermal resources of Seulawah Agam Volcano, Indonesia. Int. J. GEOMATE, vol. 17, no. 62, pp. 173–180, Oct. 2019.

[19] Ismail N., Yanis M., Idris S., Abdullah F., and Hanafiah B., Near-Surface Fault Structures of the Seulimuem Segment Based on Electrical Resistivity Model. J. Phys. Conf. Ser., vol. 846, p. 012016, May 2017.

[20] Marwan, Syukri M., Idroes R, and Ismail N., Deep and shallow structures of geothermal Seulawah Agam based on electromagnetic and magnetic data. Int. J. GEOMATE, 2019

[21] Mia M.B., Fujimitsu Y, and Nishijima J. Exploration of hydrothermal alteration and monitoring of thermal activity using multi-source satellite images: A case study of the recently active Kirishima volcano complex on Kyushu Island, Japan. Geothermics, 2019.

[22] Yanis M., Novari I., Zaini N., Marwan., Pembonan A.Y., and Nizamuddin., OLI and TIRS Sensor Platforms for Detection the Geothermal Prospecting in Peut Sagoe Volcano, Aceh Province, Indonesia. International Conference on Electrical Engineering and Informatics. IEEE, 2020.